Prepublished copy

Nature Environment & Pollution Technology

This is a peer-reviewed prepublished version of the paper to be published in Vol. 25, No. 4, December 2026 issue

Type of the Paper (Original Research)

Simulation of the Migration Law of Cr(VI) in Groundwater Using A Fully Coupled Numerical Model

Haihua Li[1,*], Gaojie Chai[1], Yahui Xu[2], Xinyi Wang[1] and Haozu Cheng[1]

[1]*School of Ecology and Environment, North China University of Water Resources and Electric Power, Zhengzhou 450046, Henan, China*

2 Huaxia Besince Environmental Technology Co. Ltd., Zhengzhou 450002, Henan, China

**Corresponding author:* Haihua Li; *lihaihua418@163.com*

Key Words	Hexavalent chromium (Cr(VI)); Solute transport; Convective dispersion; Fully coupled numerical model
DOI	https://doi.org/10.46488/NEPT.2026.v25i03.D1889 (DOI will be active only after the final publication of the paper)
Citation for the Paper	Li, H., Chai, G., Xu, Y., Wang, X., and Cheng, H., 2026. Simulation of the migration law of Cr(VI) in groundwater using a fully coupled numerical model. *Nature Environment and Pollution Technology*, 25(4), D1889. https://doi.org/10.46488/NEPT.2026.v25i03.D1889

Abstract: Coupled numerical model is widely used for the investigation of heavy metal migration in groundwater. This study selected a chromium slag stacking site in Henan Province, China, and its surrounding area as the research object to investigate the effective prevention of the pollution of soil and groundwater by hexavalent chromium (Cr (VI)), a by-product of chromium salt production. To this end, a three-dimensional numerical model of the water flow and solute transport, fully coupled with convective dispersion, was constructed. The model was employed to examine the migration patterns of Cr (VI) in soil and groundwater, while considering the influence of phreatic surface fluctuations caused by rainfall infiltration and soil matrix adsorption. The simulation results demonstrated that compared to the absence of rainfall, rainfall enhanced the convection and dispersion of groundwater flow. Consequently, this promoted the migration of Cr (VI)in the groundwater of the saturated zone, resulting in a de-crease in the concentration of Cr (VI)in the soil center of the vadose zone from 568 to 224 mg/kg within five years, and a decrease in the concentration of Cr (VI)in the groundwater of the saturated zone from 271 to 159 mg/kg. The investigation of soil adsorption revealed that the adsorption of the soil matrix can expand the range of variation in Cr (VI) concentration, while reducing the overall migration quantity compared to the absence of rainfall.

1. INTRODUCTION

The rapid urbanization and industrialization that have characterized the economic growth of China have resulted in a significant environmental concern: heavy metal pollution, particularly, chromium-based pollution, in soil and groundwater Adnan et al. (2022). In the early stages of production, the utilization rate of resources

for the preparation of chromium salt in China is relatively low, resulting in a considerable amount of solid waste Xu et al. (2006). The production of solid chromium slag waste is estimated to be in the range of 2.5 to 3 tons per 1 ton of chromium salt Dhal et al. (2013). The solid chromium slag waste generated during the industrial production process is randomly stacked in an open field. However, during storage, chromium slag continues to produce chromium slag filtrate Cao et al. (2024), Liu et al. (2022); thus, the stored heaps have resulted in significant contamination of the soil and groundwater around the stacking site. This environmental pollution poses a considerable risk to the health and well-being of local residents and the surrounding ecological environment. Therefore, it is imperative that effective prevention and control measures are implemented without delay Manisalidis et al. (2020).

COMSOL 6.4 (COMSOL Inc., Sweden, Stockholm) is a robust numerical simulation software that enables the coupling of multiple physical fields, thus facilitating the investigation of engineering optimization problems Sumit et al. (2021). The groundwater flow module is capable of simulating the application of porous media in the fields of hydrology, geotechnical engineering, and environmental science Nasir et al. (2014), Zhang et al., (2020). Particularly, it can support various mesh types, including 2D (triangle/quadrilateral) and 3D (tetrahedron/hexahedron/prism) meshes Masood & Ali (2020), enabling its use for the modeling and resolution of diverse scientific and engineering issues pertaining to partial differential equations (PDEs). The software utilizes porous media and groundwater flow modules Bai et al. (2024), Qiao et al. (2023), and studies have developed these two modules to simulate the trajectory of heavy metals in soil. For example, Xie et al. (2020). combined migration law and numerical simulation analyze the concentration of heavy metals, specifically Cd and Cu, in soil samples from a mining area. They selected the homogeneous soil of the sand dam as the research object, and quantified the total amount of pollutant migration in the dam body and the dam outlet using a prediction model developed through COMSOL. Based on the finite element COMSOL simulation platform, Li et al. (2021). developed a transient model to evaluate the relevant parameters in the transmission process by breaking through the curve. Wang et al. (2025) established a numerical simulation model of groundwater flow and solute migration model were established using GMS software, and the migration time of hexavalent chromium to the water source protected area under different scenarios was analyzed and predicted, which provided a scientific basis for the prediction and prevention of chromium pollution in the polluted site. Additionally, Liang et al. (2019). simulated the effects of the layered heterogeneous structure of soil on water and solute transport in unsaturated zone using COMSOL simulation software. Despite these studies, there is only little literature on the reaction process of Cr in contaminated sites.

In this study, the research area comprised a chromium slag stacking site and its surrounding area in Henan Province. The objective of this study was to analyze the degree of soil and groundwater contamination and the spatial distribution of Cr (VI) at the contaminated site. Direct assessment of rainwater recharge based on Estimating Groundwater Recharge (2010), assuming rainwater is the primary recharge mechanism, to this end, a three-dimensional numerical model of the actual contaminated site was constructed, and the multi-physical field coupling of water flow and solute transport was conducted using a groundwater flow model and a reactive solute transport model of porous media. This approach enabled the accurate description of the migration law of Cr (VI)

pollutants in the unsaturated zone soil and saturated zone groundwater. The findings of this study will provide a scientific basis for the adoption of effective remediation technology to protect soil and groundwater resources.

2. STUDY AREA

2.1. Geographical and geomorphological overviewSubsection

The study area is located in a northern city of Henan Province, located in the southeast of Taihang Mountain, the northern margin of the alluvial plain in the lower reaches of the Yellow River. According to the types of geomorphological causes, it is divided into three geomorphological types: structural erosion hilly land, piedmont alluvial plain and alluvial plain. The study area is a slightly inclined land, with an elevation of 73–76 m and a slope of 3%. The terrain is inclined from northwest to southeast, high in the north and low in the south. The surface lithology is silt and silty clay.

The study area is located in a warm temperate continental monsoon climate zone, characterized by hot summers, cold winters, concentrated rainfall, and distinct seasons. The long-term average temperature is 14°C, with a long-term average precipitation of 586.32 mm. Annual precipitation varies significantly, ranging from a maximum of 1375.3 mm during a wet year (2021) to a minimum of 327.7 mm during a dry year (2002). Precipitation is concentrated in July and August. The long-term average evaporation is 1772.62 mm, 3 to 4 times the precipitation amount, with June experiencing the highest evaporation. The long-term average absolute humidity is 12.9 mb, and the relative humidity is 65%.

2.2. Overview of the contaminated sites

The chemical plant in the study area produced sodium dichromate using chromium ore, soda ash, sulfuric acid, dolomite, and limestone as raw materials. The plant area has become a storage site for chromium slag produced during the previous production (chromium slag composition as shown in Table 1), covering an area of 4230 m^2. From 2009 to 2015, the chromium slag and chromium pollutants in the plot were treated and landfilled, after which the treatment equipment was removed, and the contaminated plot was left idle until now.

Table 1: List of chromium slag components in chemical plants.

Component	Cr_2O_3	Fe_2O_3	Al_2O_3	SiO_2	MgO	CaO	Water-soluble chromium	acid soluble chromium	pH value
Content	5.48%	8.46%	8.20%	8.91%	22.41%	32.46%	0.39%	0.47%	>10

3. RESEARCH METHODOLOGY

3.1. Basic equation of groundwater flow

Combined with the hydrogeological conditions of the contaminated site in the study area, this study selected the unsaturated seepage continuity equation-Richards equation to describe the three-dimensional movement of water in the saturated zone and the unsaturated zone De Smedt (2016), Song & Borja (2014), and Therrien & Sudicky (1996), the basic equation is as follows.

$$\rho\left(\frac{C_m}{\rho g}+S_e S\right)\frac{\partial p}{\partial t}+\nabla\bullet\rho\left(-\frac{k_s}{\mu}k_r\left(\nabla p+\rho g\nabla D\right)\right)=Q_m \tag{1}$$

In the formula: ρ is the density of the fluid, kg/m^3; p is the pressure head, Pa; S is the water storage coefficient, 1/m; C_m for water capacity， when the soil is saturated C_m is 0,1/m; S_e is the effective saturation of the soil, when the soil is in a saturated state 1; k_s is the permeability of soil in saturated state, m/s; k_r is relative permeability, in unsaturated soils, k_r is a function of effective saturation; γ bulk density of fluid, kg/(m·s)^2; D for elevation, m; Q_m for the source sink term, it represents the inflow of fluid per unit volume per unit time under external conditions such as rainfall infiltration, and the unit is kg/(m^3·s);

Among them, in the unsaturated state, the soil moisture content θ、C_m、S_e and k_r can be made by Van Genuchten the retention model is obtained (2010), and the calculation equation is as follows:

$$\theta=\theta_r+Se(\theta_s-\theta_r) \tag{2}$$

$$C_m=\frac{\alpha m}{1-m}(\theta_s-\theta_r)Se^{\frac{1}{m}}(1-Se^{\frac{1}{m}})^m \tag{3}$$

$$Se=\frac{1}{[1+|\alpha H_p|^n]^m} \tag{4}$$

$$k_r=Se^L[1-(1-Se^{\frac{1}{m}})^m]^2 \tag{5}$$

In the formula: θ_s is the soil moisture content in saturated state; θ_r is the residual moisture content after soil drainage; α, m, n is the constitutive relation constant of the model, where $n = 1/m$； H_p the matrix potential of the soil is negative, m.

3.2. Pollutant transport control equation

Considering the influence of convection, dispersion of groundwater flow and adsorption of pollutants by soil matrix in the study area Anderson et al. (1979) and Banaei et al. (2021), a three-dimensional solute transport partial differential equation of convection-dispersion-adsorption-reaction is established to describe Cr(VI) the basic governing equations for migration in saturated and unsaturated zones are as follows:

$$\frac{\partial}{\partial \mathrm{t}}(\theta_l C_i)+\frac{\partial}{\partial t}(\rho C_{p,i})+\frac{\partial}{\partial t}(\theta_g C_{G,i})+u\bullet\nabla C_i=\nabla\bullet[(D_{D,i}+D_{e,i})\nabla C_i]+R_i+S_i \tag{6}$$

In the formula, the left side of the equation is the concentration change of the substance in the liquid phase, solid phase and gas phase, respectively. The fourth term represents the convective transfer of solute under the action of groundwater velocity field; C_i indicates the concentration of solute in the liquid phase, the unit is mol/m^3, $C_{p,i}$ indicates the amount adsorbed on the solid particles, the unit is mol/(ρ_s g), $C_{G,i}$ denotes the concentration of a substance in the gas phase. In this study, the volatilization of the gas phase is not considered, and

the concentration value is 0; u is the groundwater flow rate, the unit is m/s; D_D represents diffusion tensor, unit is m^2/s, D_e indicates the effective diffusion coefficient, the unit is m^2/s. R_i is the expression of reaction rate, representing the chemical reaction of a substance in a liquid or solid phase; S_i represents the sink source term, and the material flows in and out with the liquid; θ_l is the volume content of the liquid, for saturated porous media θ_l = porosity ε, for unsaturated porous media, liquid volume fraction $\theta_l = \varepsilon \times S$, S for soil saturation.

The main factors affecting the transport of soil groundwater solute are convection, hydrodynamic dispersion, adsorption and chemical reactions of various sink source terms.

3.3. Hydrogeological conceptual model of the study area

3.3.1. Study area generalization

In this study, the simulation range was determined by the mainstream diameter direction of groundwater flow and the distribution of boreholes. The simulation range of the contaminated sites is shown in Fig. 1.

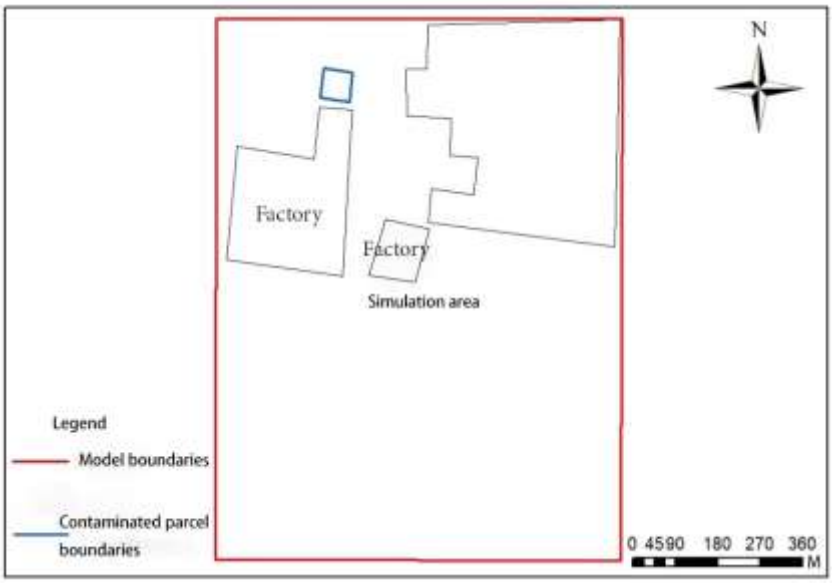

Fig. 1: Model simulation scope plan.

3.3.2. Model boundary condition generalization

（1）Model lateral boundary condition generalization

Owing to the incomplete hydrological unit in the study area and the lack of specific supply and discharge data, the general water level contour was used as the general head boundary Costabile et al. (2019) and Miller et al. (2013), and the simulation was consistent with reality to improve the accuracy of the model.

（2）Model vertical boundary condition generalization

Based on the data from 71 boreholes, a three-dimensional geologic model was constructed using Arcgis 10.8.2(Environmental Systems Research Institute, Inc., Red-lands, California, USA) software for interpolation and then imported into COMSOL. The surface was the upper boundary and the lower silty clay, which is divided into six layers, was the lower boundary. The six layers includes the unsaturated zone, which is divided into two

layers, and the. saturated zone, which is divided into four layers, including the shallow aquifer, the first aquifer (fine sand), the weakly permeable layer (silty clay), and the second aquifer (fine sand). Beneath the second aquifer is a thick silty clay aquiclude. The model utilized rainfall recharge, considers the difference be-tween multi-year rainfall and evaporation, and the water flow is mainly southeast-ward.

3.3.3. Numerical model mesh generation

In this study, the groundwater flow movement and solute transport in the study area were simulated using the groundwater flow module and the porous media dilute transport module of COMSOL software. The developed three-dimensional geological model was divided into several units using a free tetrahedral mech. Additionally, the model was divided into six layers in the vertical direction, adding up to a total of 808,267 tetrahedral mesh units, 24 vertex units, and 2718 edge units. The total volume of the mesh was 7348 × 107 m^3. The mesh generation of the model is shown in Fig. 2.

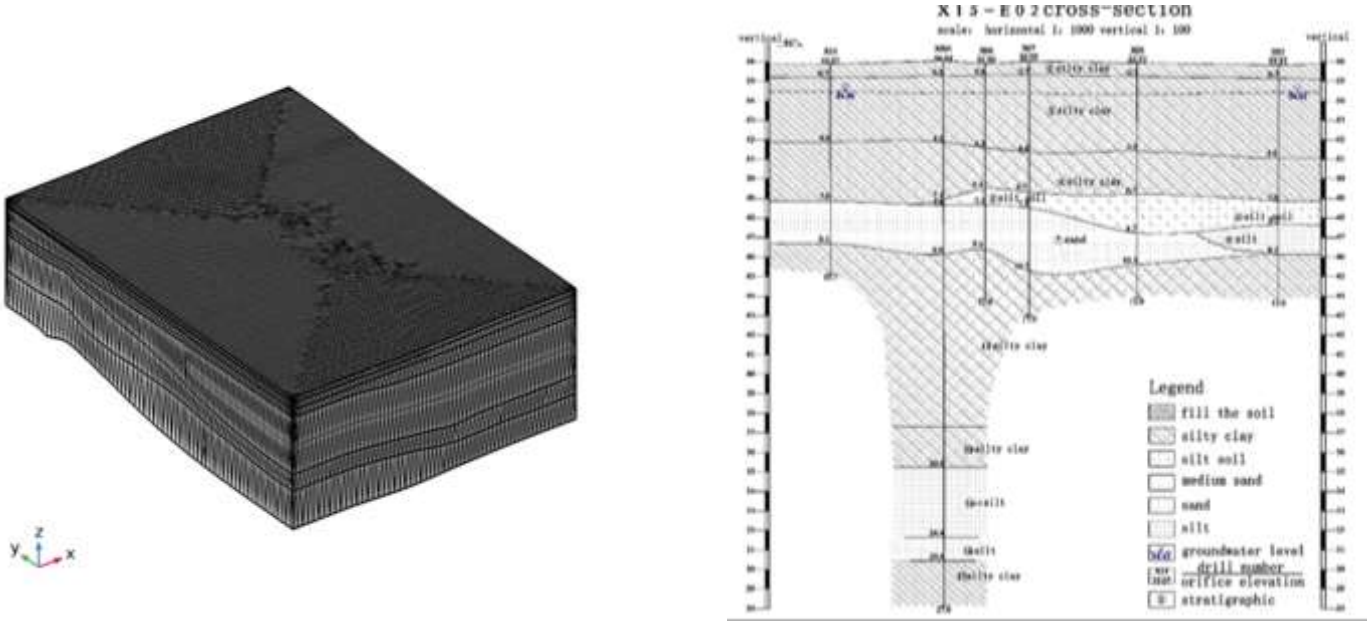

Fig. 2: Three-dimensional model mesh segmentation diagram and cross-sectional view

3.4. Model validation

The performance of the model Thanh et al. (2022), Tian-chyi et al. (2015) was validated to determine its ability to accurately reflect the geological characteristics and groundwater flow movement in the study area, and provide a basis for the accurate numerical simulation of subsequent soil groundwater solute transport.

By inputting the field data, first, the model performs a steady-state simulation, after which it was repeatedly calibrated to ensure that the simulated groundwater level is consistent with the actual measurement. The selected groundwater monitoring wells are shown in Fig. 3, where JA represents the first aquifer monitoring well and JB represents the second aquifer monitoring well. Table 2. presents the fitting result of the water level after the simulation calculation. The comparison of the simulated and actual value revealed that the error between the simulated value of the groundwater level of the first and second aquifers and the actual monitoring value is small, and that the agreement is good. The variance sum of squares error (SSE), mean square error (MSE), and

root mean square error (RMSE) of the simulated value of the groundwater level of the first aquifer and the measured value were 0.567 m^2, 0.0945 m^2 and 0.3074 m, respectively, and those of the simulated value of the groundwater level of the second aquifer and the measured value were 1.101 m^2, 0.1834 m^2 and 0.4283 m, respectively, indicating the consistency between the initial flow field of the model and the actual hydrogeological conditions of the study area. Through the cloud map of groundwater level distribution established in Fig. 4, the height of groundwater level in the aquifer gradually decreases from south to north, which is consistent with the actual hydrogeological survey results. This confirms that the model can reflect the flow field characteristics of the actual site, and the steady flow field of this simulation can be used as the initial flow field of the unsteady flow simulation.

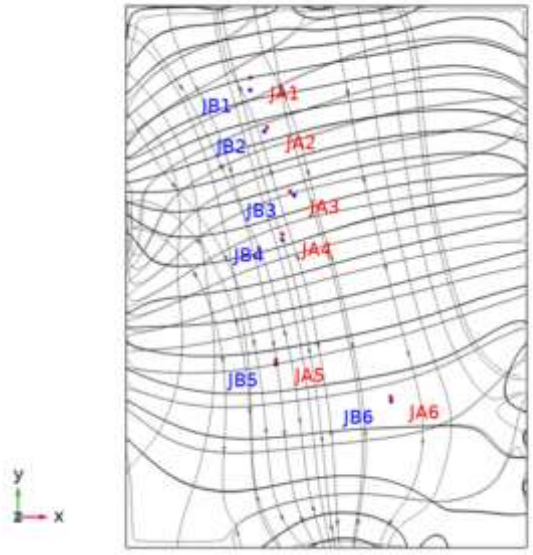

Fig. 3: Distribution map of groundwater monitoring wells in different aquifers.

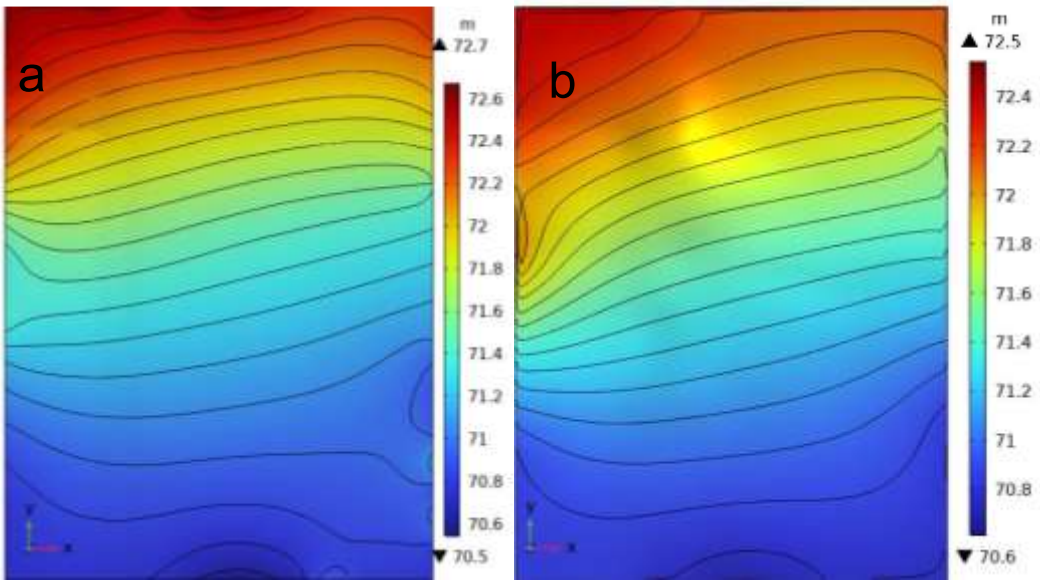

Fig. 4: Cloud map of groundwater level distribution in different aquifers and water level contour map, (a) first aquifer; (b) second aquifer.

Table 2: Statistical analysis results of errors between calculated water levels and actual observed water levels at different points.

Study area aquifer	Monitoring wells	Simulated water level (m)	The actual monitoring water level (m)	Absolute error value of water head (m)
First aquifer	JA1	72.41	72.65	0.24
	JA2	72.20	72.42	0.22
	JA3	71.50	71.88	0.38
	JA4	71.11	70.93	0.18
	JA5	71.00	70.79	0.21
	JA6	69.84	70.33	0.49
Second aquifer	JB1	72.29	72.40	0.11
	JB2	72.15	72.60	0.45
	JB3	71.93	73.10	1.17
	JB4	71.15	70.9	0.25
	JB5	70.98	70.79	0.19
	JB6	70.63	70.51	0.12

3.5. Determination of solute transport related parameters

This study investigates the migration pattern of Cr (VI) in soil and groundwater systems in chromium slag stacking contaminated sites. From the parameters of soil physicochemical properties in the study area obtained from the geotechnical tests, a total of five geotechnical sampling points were deployed with reference to the national norms Standard for geotechnical testing method (GB/T 50123) and Standard for test methods of engineering rock mass (GB/T 50266). Soil physical property parameters such as water content, porosity, bulk weight (g/cm^3), saturation, etc., were obtained through geotechnical tests, and some of the geotechnical test results are shown in Table 3. This study adopted the solute transport model of un-steady flow, and the model considered factors, such as convection, dispersion, adsorption, and chemical reaction. The simulation time was 1800 d, for each stress period per day and the simulation step size was controlled using a Time-Dependent Solver mod-ule, follow the error control principle to ensure numerical stability. According to the type of contaminated sites, diffusion coefficient, dispersion, equilibrium adsorption constant, and maximum adsorption capacity of soil to Cr (VI) were based on the values of relevant parameters in the study of Cr (VI) transport and transformation mechanism in chromium slag contaminated sites by Paolina et al. (2023) and He et al. (2022). The identified parameters for identification verification are shown in Table 4.

Table 3: Geotechnical test results.

Sample Number	Sample Type	Sampling Depth	Bulk Weight	Porosity (%)	Saturation (%)
TG16	fill the soil	0–1 m	1.53	44.77%	43.23
	silty clay	2–6 m	1.64	34.55%	82.21
	sand	8–12 m	1.40	56.11%	100
TG04	fill the soil	0–1 m	1.77	47.33%	52.33
	silty clay	2–6 m	1.53	36.68%	100
	sand	8–12 m	1.44	58.28%	100

Table 4: Identification results of hydrogeological parameters.

Parameters	Unsaturated Zone			Saturated Zone		
	First Layer	Second Layer	Third Layer	Fourth Layer	Fifth Layer	Sixth Layer
Kxx (cm/s)	2.3 × 10−4	2.7 × 10−5	2.7 × 10−5	9 × 10−4	2.7 × 10−5	9 × 10−4

Parameters	Unsaturated Zone		Saturated Zone			
	First Layer	Second Layer	Third Layer	Fourth Layer	Fifth Layer	Sixth Layer
Kyy (cm/s)	2.3 × 10−4	2.7 × 10−5	2.7 × 10−5	9 × 10−4	2.7 × 10−5	9 × 10−4
Kzz (cm/s)	2.3 × 10−4	2.7 × 10−5	2.7 × 10−5	9 × 10−5	2.7 × 10−6	9 × 10−5
Porosity ε	0.43	0.37	0.37	0.57	0.37	0.57
Saturated water content θs	0.43	0.37	/	/	/	/
residual water content θr	0.05	0.1	/	/	/	/
a	1.2	0.5	/	/	/	/
n	3	1.09	/	/	/	/
Soil density ρs (kg/m^3)	1530	1550	1550	1420	1550	1420

4. RESULTS AND DISCUSSIONS

4.1. Analysis of Cr(VI) migration in industrial contaminated sites

4.1.1. Analysis of the influence of rainfall recharge on Cr(VI) migration

(1) Distribution of Cr(VI) initial pollution range in the study area

The distribution of Cr (VI) in the plane and the three-dimensional initial concentration field of Cr (VI) in the industrial contaminated site obtained through model simulation are presented in Fig. 5 and 6. In the plane contamination area distribution cloud map, the y-axis is in the north direction. Fig. 5 reveals that while the Cr (VI) concentration in the vadose zone soil is locally too high, the aquifer groundwater in the downstream vadose zone soil is not polluted by Cr (VI). Fig. 6 reveals that highly polluted groundwater is mainly distributed in the chrome slag dump and the downstream area near the chrome slag dump.

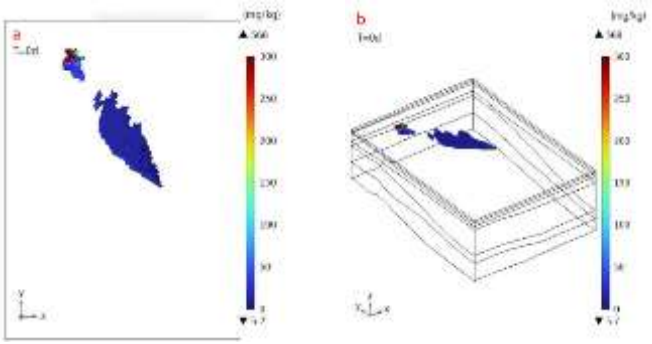

Fig. 5: Distribution map of Cr(VI) initial pollution plume in the vadose zone (a: Plan view; b: 3D view).

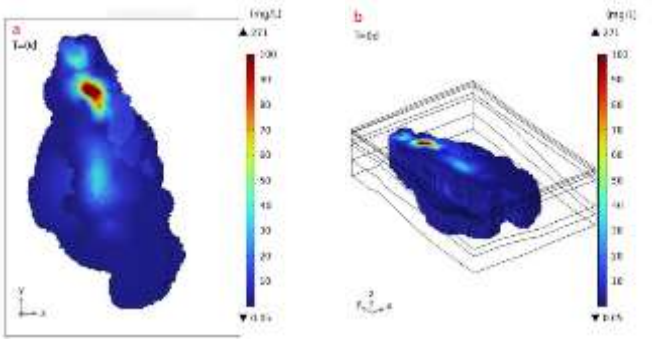

Fig. 6: Initial Cr (VI) pollution plume distribution map of groundwater (a: Plan view; b: 3D view).

(2) Comparison and analysis of the distribution of Cr (VI) in contaminated sites under different rainfall recharge condition.

In the absence of rainfall infiltration, the Cr (VI) concentration in the soil center of the vadose zone of the contaminated site decreased from 568 to 224 mg/kg within 5 years (Fig. 7). Similarly, in the presence of rainfall infiltration, the concentration of Cr (VI) in the soil center of the vadose zone in the contaminated site decreased from 568 to 307 mg/kg within 5 years (Fig. 8). Additionally, the concentration of Cr (VI) in the soil exhibited a fluctuating trend, and the pollution plume increased and moved downstream along the groundwater flow. The comparison of the two conditions under which the plume was simulated revealed that the fluctuation of the phreatic surface caused by rainfall infiltration expands the area of soil contamination in the vadose zone and induces an increase in the Cr (VI) contaminant content in the vadose zone.

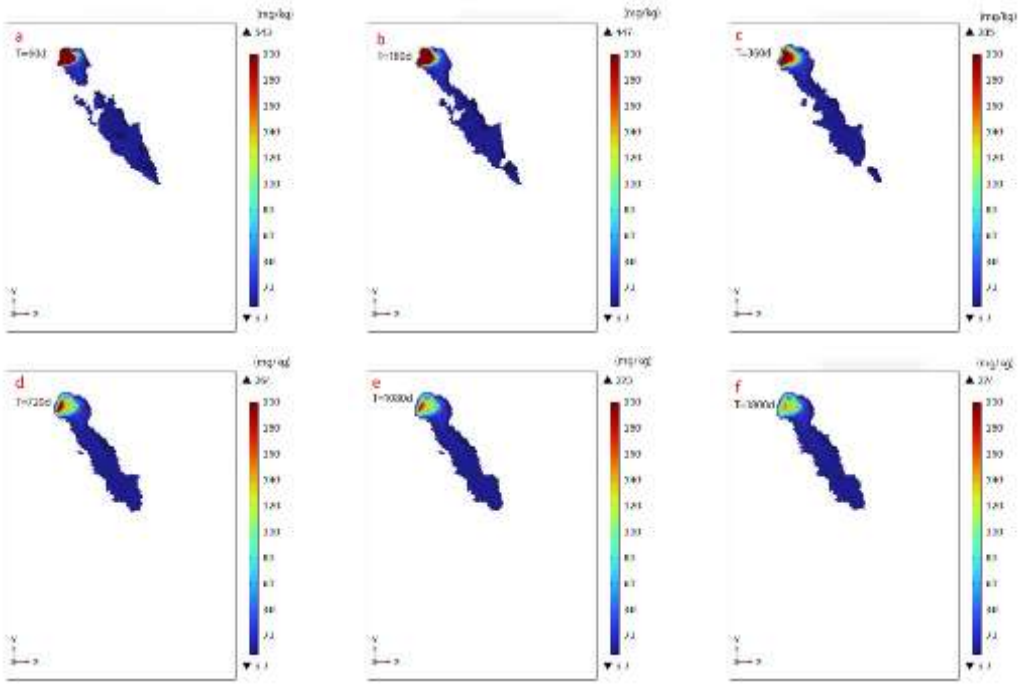

Fig. 7: Cloud map of pollution plume distribution of Cr (VI) in aerated zone under non-rainfall recharge and leaching. (a) 60 d; (b) 180 d; (c) 360 d; (d) 720 d; (e) 1080 d; (f) 1800 d.

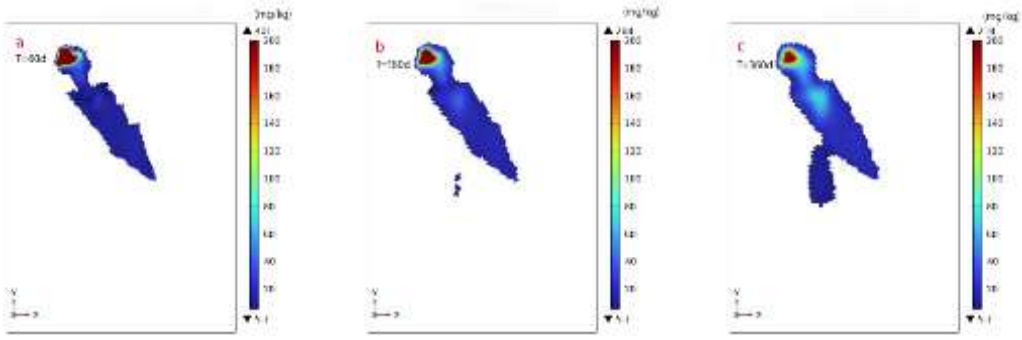

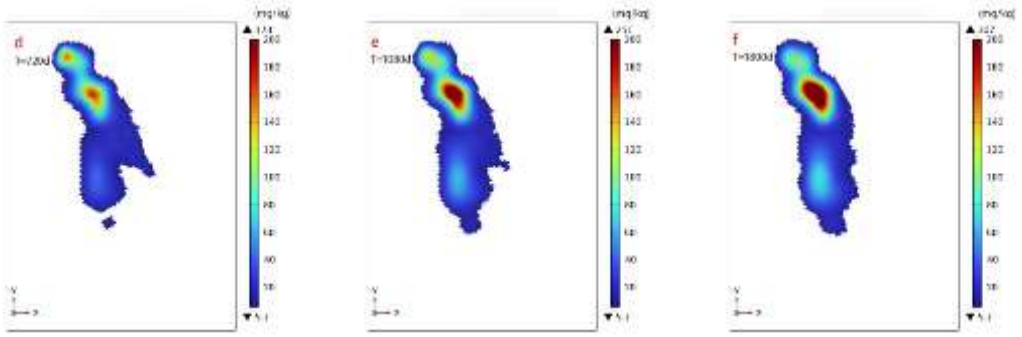

Fig. 8: Cloud map of pollution plume distribution of Cr (VI) in aerated zone under rainfall re-charge and leaching. (a) 60 d; (b) 180 d; (c) 360 d; (d) 720 d; (e) 1080 d; (f) 1800 d.

In the absence of rainfall infiltration, the concentration decreased to 182 mg/L (Fig. 9) only through convection and dispersion, whereas the center concentration of the plume decreased to 159 mg/L (Fig. 10) under the effect of rainfall. In contrast, rainfall leaching expands the area of contamination, indicating that rainfall can pro-mote the release of chromium pollutants from the vadose zone soil to the aquifer and accelerate the migration of Cr (VI) between the two. When considering the recharge and leaching of rainfall infiltration, the area of the groundwater pollution plume in the saturated zone increases, the pollution area expands to the upstream area, and the central concentration decreases more significantly, indicating that rainfall infiltration can enhance the convection and dispersion of groundwater flow, thus worsening the pollution degree of soil and groundwater

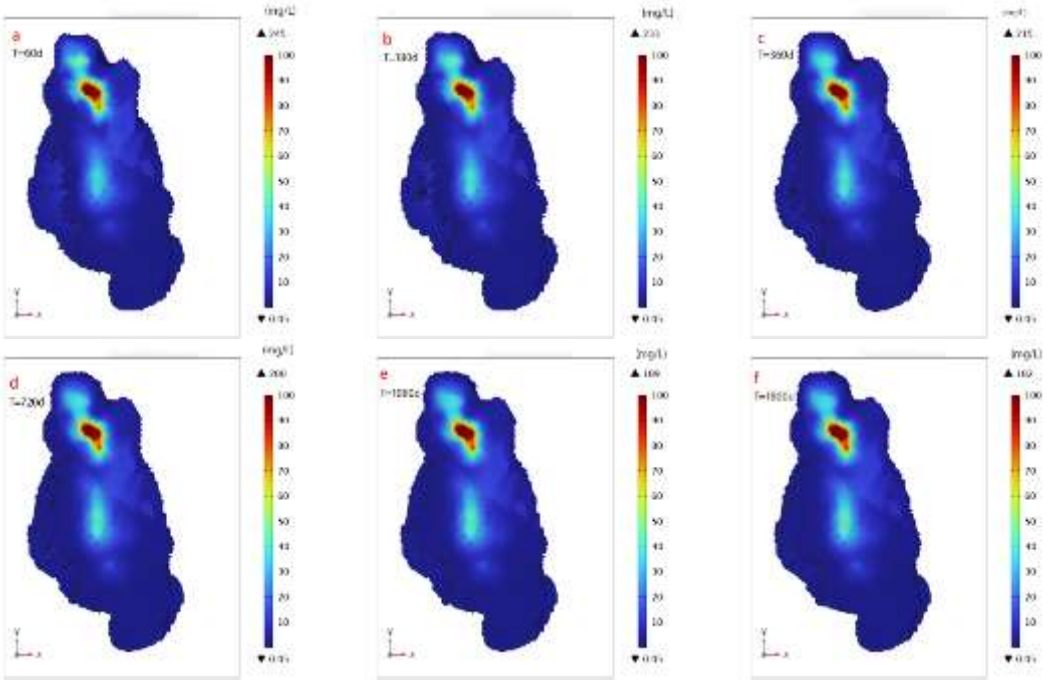

Fig. 9: Cloud map of Cr (VI) pollution plume distribution of groundwater under no rainfall recharge and leaching. (a) 60 d; (b) 180 d; (c) 360 d; (d) 720 d; (e) 1080 d; (f) 1800 d.

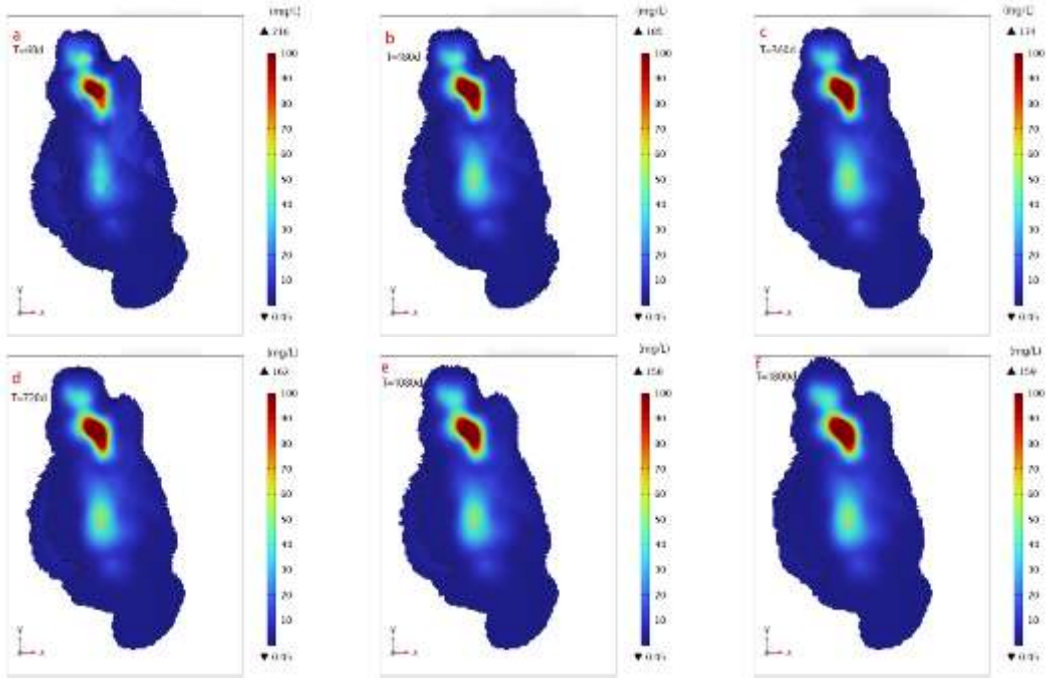

Fig. 10: Cloud map of Cr (VI) pollution plume distribution of groundwater under rainfall recharge and leaching. (a) 60 d; (b) 180 d; (c) 360 d; (d) 720 d; (e) 1080 d; (f) 1800 d.

(3) Analysis of the variation characteristics of Cr (VI) concentration at different depths of the vadose zone in the presence and absence of rainfall recharge.

The migration of Cr (VI) in the contaminated site along the upstream, middle, and downstream of the groundwater flow direction was marked as D01, D02 and D03 points (Fig. 11). In the absence of rainfall, the migration of Cr (VI) was influenced by capillary action and molecular diffusion of soil moisture in the unsaturated zone. The comparison of the soil depth data of the three sites revealed that the Cr (VI) concentration was higher in the upper layer of the vadose zone, but lower in the lower layer. Additionally, along the direction of the groundwater flow, the concentration of Cr (VI) in the upper layer of D02 and D03 increased, whereas that in the lower layer decreased. Over time, the concentration of Cr (VI) at different depths of each point tends to stabilize, which can be mainly attributed to the diffusion of Cr (VI) in the high-concentration area to the low-concentration area under capillary action, resulting in a gradual decrease in its concentration.

In the presence of rainfall leaching, the concentration of Cr (VI) in the surface soil decreased significantly with rainfall leaching in the upstream D01 point, whereas the concentration of Cr (VI) increased in all positions in the downstream D02 and D03. Compared to the absence of rainfall, rainfall infiltration significantly affected the migration of Cr (VI) in the soil. The concentration of Cr (VI) in the upstream surface layer decreased and slightly increased at the depth of 3.5 m, while the downstream soil mi-grated to the upper layer through leaching and diffusion, causing groundwater pollution and triggering water convection in the vadose zone Consequently, this resulted in the movement of Cr (VI) in the vadose zone to the downstream soil. The increase in the Cr (VI) concentration in the upper soil was greater than that in the lower soil, and this can be mainly attributed to the less effect of the fluctuation of the groundwater level on the soil at a depth of 3.5 m, and the flow of the Cr (VI)

in the surface soil to the lower layer through evaporation and migration, resulting in greater concentration fluctuation.

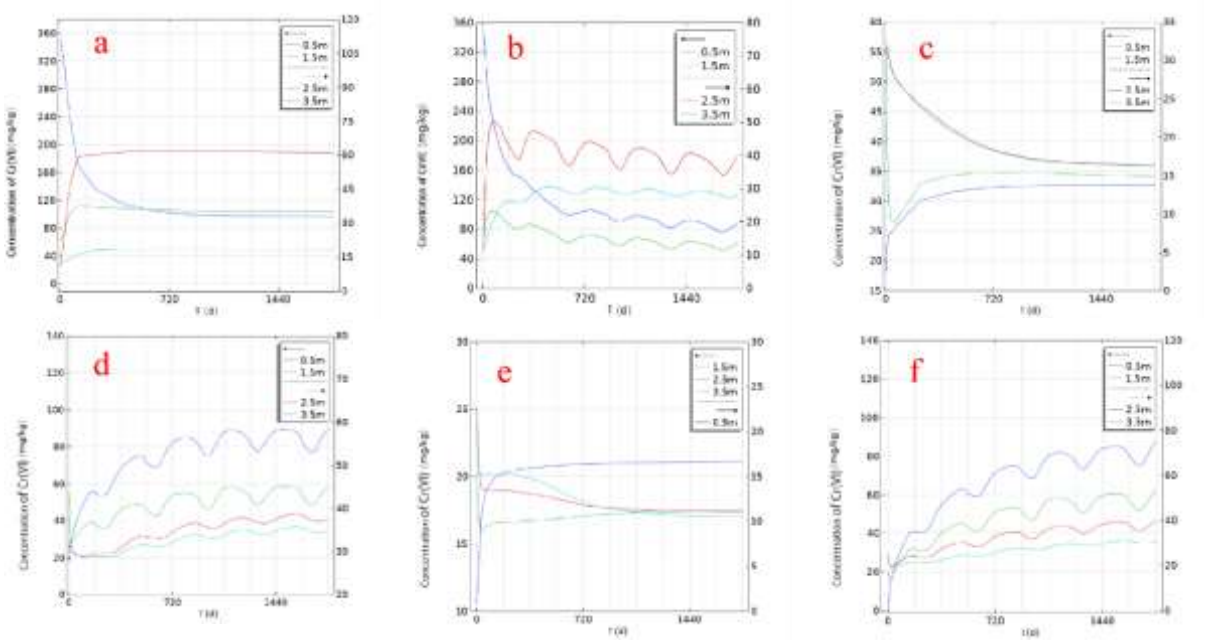

Fig. 11: Changes in Cr (VI) concentration at different depths in the vadose zone of polluted land under rainfall leaching. (a) D01 point without rainfall; (b) D01 point under rainfall; (c) D02 point without rainfall; (d) D02 point under rainfall; (e) D03 point without rainfall; (f) D03 point under rainfall.

(4) Examination of the variation in Cr(VI) concentration in groundwater with and without rainfall recharge in different aquifers

In the absence of rainfall recharge leaching, the concentration of Cr (VI) in up-stream wells (Fig. 3) JA1, JA2, JA4 (in a high concentration gradient) decreased owing to convection and dispersion. Despite its position below the pollution source, the recharge of clean groundwater decreased (Fig. 12) the overall concentration of the contaminant. The concentration of contaminants in groundwater at monitoring wells JA5 and JA6, situated along the downstream trajectory of the groundwater flow, in-creased owing to the influence of upstream polluted water. Similarly, JA3 is situated in the middle reaches, which are subject to the convection and dispersion of the first aquifer, and the water flow in the highly polluted area migrates towards the middle reaches. In the context of rainfall recharge leaching, the observed variation trend in Cr (VI) concentration across monitoring wells was consistent with that observed in the absence of rainfall. However, a notable distinction was observed in the concentration profiles of the monitoring wells situated in proximity to the center of the pollution plume, which exhibited a gradual decline, whereas those located downstream demonstrated a rapid increase. This phenomenon can be attributed to the enhanced supply of soil to groundwater Cr (VI) and the weakened degradation of high-pollution areas, which are both influenced by rainfall.

Under the two conditions, there was no significant change in the concentration of Cr (VI) in the groundwater monitoring well of the second aquifer. Under rainfall re-charge leaching, the concentration of Cr (VI) in the high-value contaminated wells JB2 and JB4 decreased, and the concentration of Cr (VI) in the upstream JB1, midstream JB3 and downstream JB5 also decreased, which was contrary to the trend of monitoring wells near

the first aquifer. This was attributed to the weak permeable layer above the second aquifer. Rainfall enhances convection and dispersion, resulting in the faster Cr (VI) flow attenuation in the second aquifer compared to downward infiltration, enhanced diffusion, and weakened aggregation. As the upstream and downstream of the contaminated plot, JB1 continued to receive groundwater recharge from the upstream high-contaminated area, thus increasing the Cr (VI) concentration.

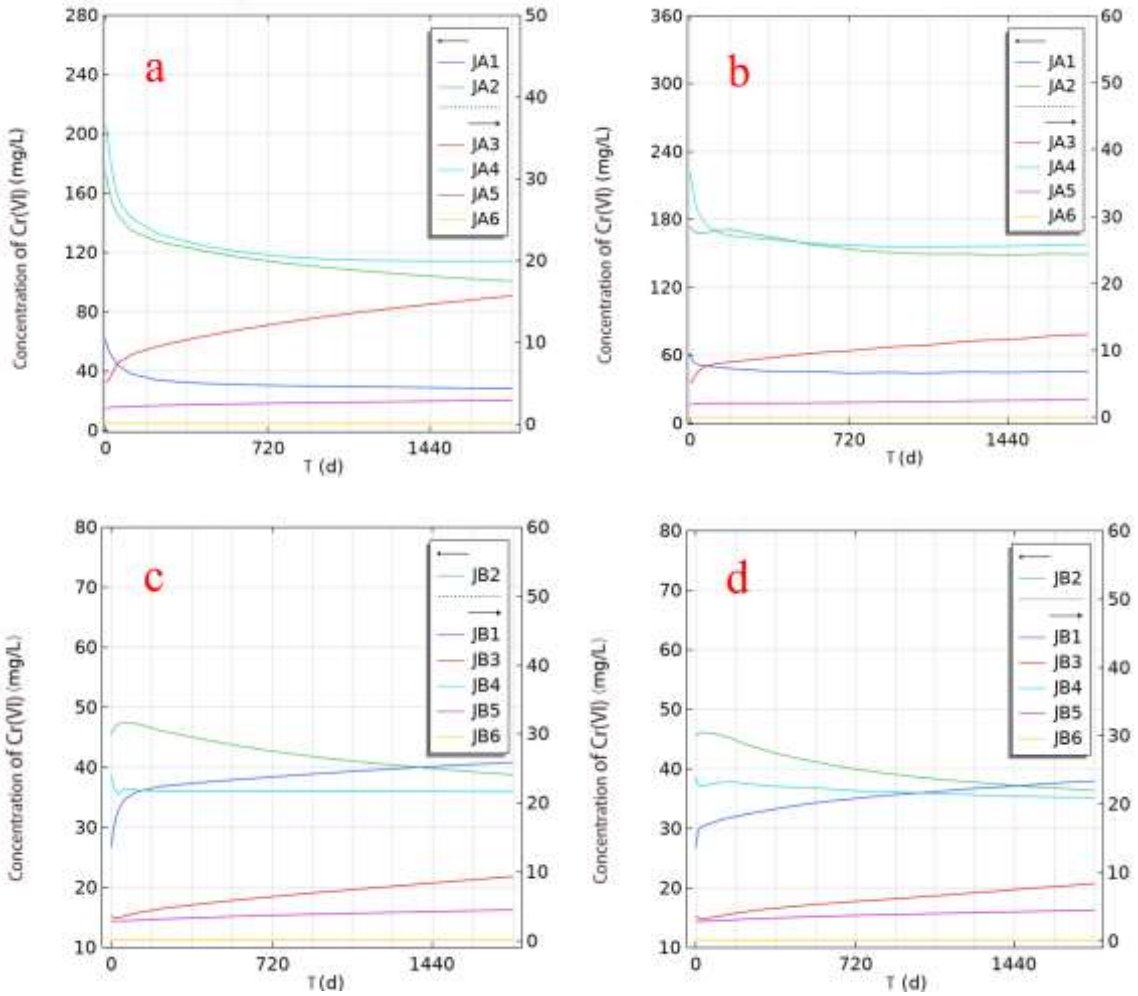

Fig. 12: Changes in hexavalent chromium concentration in groundwater at different points in the aquifer under rainfall leaching. (a) the first aquifer without rainfall; (b) the first aquifer under rainfall; (c) the second aquifer without rainfall; (d) the second aquifer under rainfall.

4.1.2. Analysis of the migration of Cr (VI) under the adsorption of soil matrix

The adsorption coefficient utilized in the simulation was based on the findings of previous experimental research on the adsorption of Cr (VI) by silty clay in the vadose zone and fine sand soil in the saturated zone. The adsorption distribution coefficient utilized in the model was based on the study of previous experimental research Liu et al. (2018), Cao et al. (2021) and Wang et al. (2000), which investigated the adsorption of Cr (VI) in diverse lithologic soils under constant temperature conditions. The distribution coefficient of fine sand lithologic soil was 0.11 L/kg, whereas that of silty clay lithologic soil was 2.63 L/kg. The results of the numerical simulation are analyzed as follows:

(1) Analysis of the variation characteristics of Cr (VI) concentration at different soil depths in the vadose zone under adsorption.

Compared to under the absence of rainfall (Fig. 13), in the presence of rainfall, the concentration of Cr (VI) in the initial soil changed rapidly owing to migration and molecular diffusion within the high concentration area. Adsorption facilitates the rapid and stable accumulation of Cr (VI), resulting in a higher concentration after stabilization than in the absence of adsorption. In the absence of precipitation and under conditions of adsorption, there was an increase in the concentration of Cr (VI) in the vadose zone at varying depths upstream of D01 point, indicating that the adsorption process enhanced the retention of Cr (VI) in the soil. The reduction in the concentration of Cr (VI) in the deep soil at D02 and D03 points was less pronounced, suggesting that adsorption impeded the migration of highly contaminated soil to the downstream area. This process also enhanced the retention of Cr (VI) in the downstream soil and reduced its diffusion to the downstream vadose zone.

Compared to rainfall conditions, in the absence of rainfall, the range of variation in Cr (VI) concentration in the soil at D01, D02 and D03 points demonstrated a reduction in variability and an increase in peak value under adsorption. This suggests that adsorption enhanced the retention of Cr (VI) in soil, thereby limiting its vertical and horizontal migration. During the wet season, the soil exhibited a greater capacity for Cr (VI) adsorption in groundwater, resulting in a higher peak value than that observed during rainfall recharge. During dry season, the adsorption process effectively blocks the diffusion of Cr (VI) in the soil, resulting in a slower rate of decline in the peak con-centration. Additionally, adsorption reduces the amount of migration between different soil depths, thereby limiting the concentration change at each point. Particularly, at 0.5 m downstream, the strong adsorption of surface soil prevents the downward diffusion of Cr (VI) in the upstream high-pollution area. Furthermore, the adsorption of deep soil limits the upward migration of Cr (VI). Ultimately, the accumulation of Cr (VI) in the surface soil is reduced.

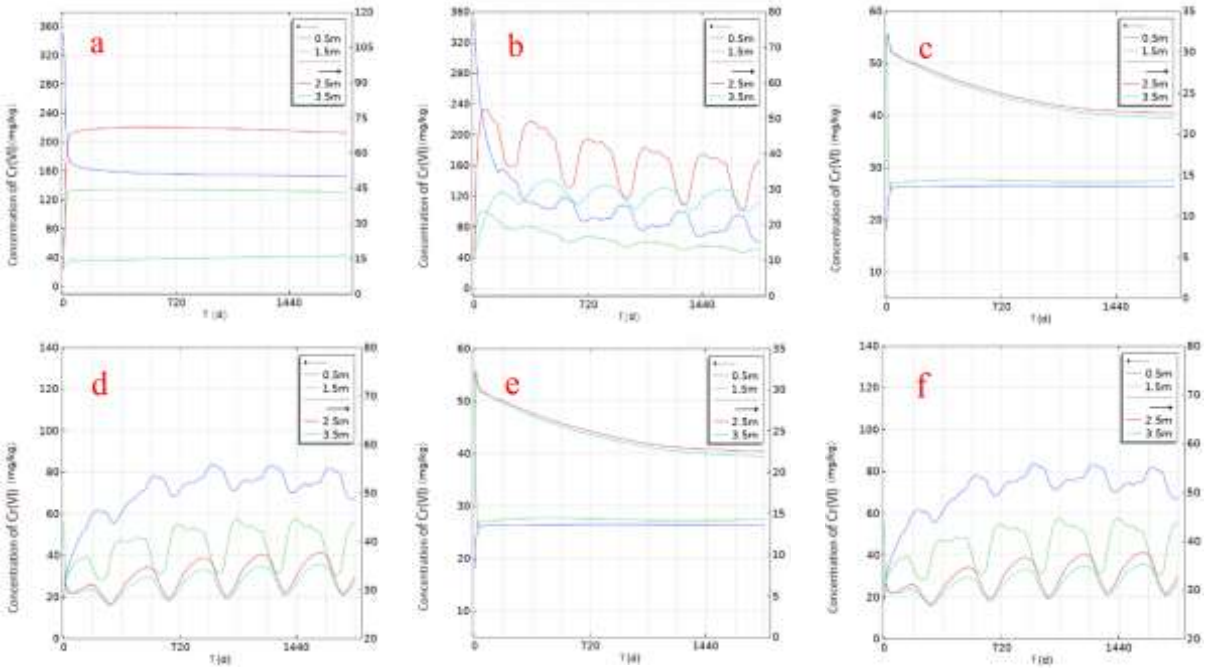

Fig. 13: Consider the changes in concentration of hexavalent chromium at different depths in the vadose zone within the polluted plot under adsorption. (a) D01 point under adsorption; (b) D01 point under rainfall adsorption; (c) D02 point under adsorption; (d) D02 point under rainfall ad-sorption; (e) D03 point under ad-sorption; (f) D03 point under rainfall adsorption.

(2) Analysis of the variation characteristics of Cr(VI) concentration in aquifer groundwater considering adsorption

The simulation results depicted in Fig. 14 demonstrate that the reduction in Cr (VI) concentration in the JA1, JA2 and JA4 monitoring wells within the initial aquifer was mitigated when the influence of adsorption was considered. This observation suggests that the adsorption of fine sand soil exerts a hindering effect on the migration process within the initial aquifer. The concentration increase in the JB1 well in the second aquifer was observed to decrease owing to the strong adsorption of Cr (VI) by the aquitard between the first and second aquifers. This limited the migration of Cr (VI) from the first aquifer to the second aquifer. Similarly, in the JB2 and JB4 monitoring wells of the second aquifer, a decrease in the Cr (VI) concentration was observed, indicating that adsorption impeded migration in the second aquifer. Generally, adsorption plays a significant role in blocking the migration of contaminants between the two aquifers.

In consideration of the adsorption, a decline in the Cr (VI) concentration in the initial aquifer (JA1, JA2 and JA4) wells was observed, as well as a reduction in the Cr (VI) concentration in JA3 and JA5 wells. This indicates that the adsorption process weakened the migration of Cr (VI) in the initial aquifer. As precipitation levels increased, the Cr (VI) adsorbed by the soil through the convection and diffusion of groundwater undergoes fluctuations, resulting in corresponding fluctuations in the concentration curve. In the second aquifer, the change range of the initial stage was smaller than that under the rainfall condition, indicating that the adsorption reduces the extent of migration. Regardless of rainfall, the Cr (VI) concentration in the second aquifer remained relatively constant after adsorption. This may be attributed to the fact that adsorption inhibits the convection and diffusion caused by rainfall, thereby decreasing the migration of Cr (VI).

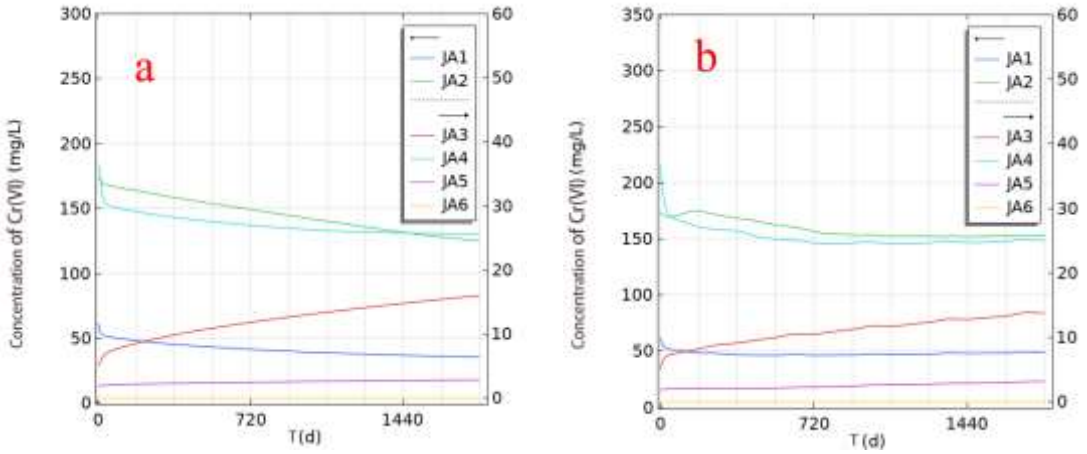

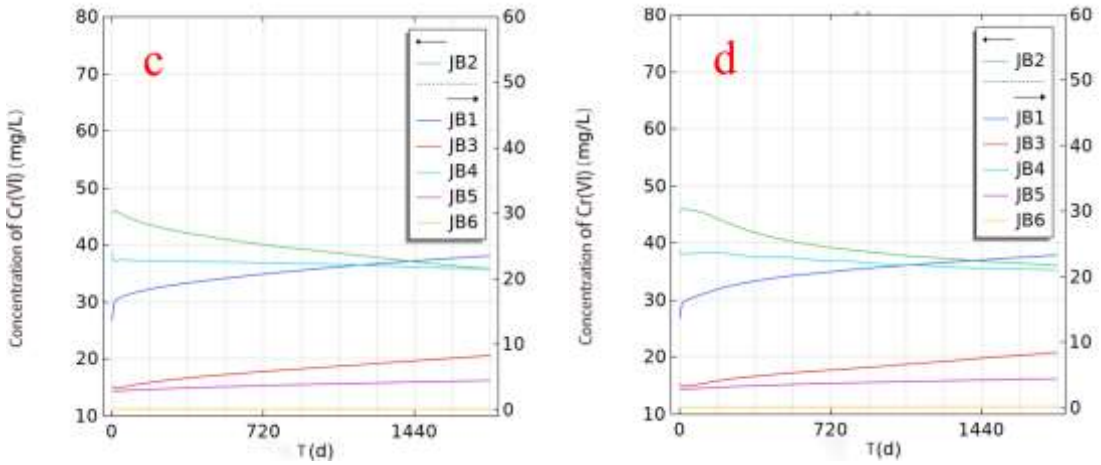

Fig. 14: Consider the changes in hexavalent chromium concentration in groundwater at different points of the aquifer due to adsorption. (a) the first aquifer under adsorption; (b) the first aquifer under rainfall adsorption; (c) the second aquifer under adsorption; (d) the second aquifer under rainfall adsorption.

5. CONCLUSIONS

This study analyzed the migration pattern of Cr (VI) in soil and groundwater under the influence of phreatic surface fluctuation and soil matrix adsorption caused by rainfall infiltration by constructing a three-dimensional fully coupled numerical model. The main conclusions are as follows:

The chromium slag contaminated site in the study is a contaminated land, and in the management process, it is necessary to strictly follow the Henan Province soil environment management measures for contaminated land (for trial implementation), to determine the responsibility of the main body to carry out the relevant investigation, assessment and remediation, and the results of the simulation study can provide data support and decision-making basis for these practical work.

The results of the simulation demonstrated that the fluctuations in groundwater levels owing to rainfall, infiltration, recharge, and evaporation exerted a considerable influence on the concentration of Cr (VI) in the vadose zone soil, particularly compared to conditions without rainfall. The variation in the Cr (VI) concentration in the vadose zone soil was consistent with the variation in the groundwater level, which facilitates the migration of Cr (VI) between the saturated zone and the unsaturated zone. Concurrently, precipitation infiltration facilitates the migration of Cr (VI) in the vadose zone soil to the aquifer groundwater. Furthermore, it will reinforce the convection of groundwater in the primary and secondary aquifers within the study area and augment its diffusion level in groundwater; thus, exacerbating groundwater Cr (VI) pollution.

It is evident that matrix adsorption exerts a discernible retardation effect on Cr (VI) in the vadose zone soil and groundwater aquifers. Compared to conditions with-out precipitation, matrix adsorption can amplify the fluctuations in Cr (VI) concentration observed in vadose zone soil. Additionally, the overall migration of Cr (VI) across different soil depths, influenced by changes in the phreatic surface due to rainfall, was diminished.

Furthermore, the retardation resulted in a certain degree of fluctuation in the variation curve of Cr (VI) concentration at different points in the first aquifer of the groundwater, which diminished the impact of convection and molecular diffusion in the second aquifer under rainfall conditions.

Authors Contributions: Haihua Li: Conceptualization, Writing – review and editing, Supervision, Resources. Gaojie Chai: Visualization, Data curation, Formal analysis, Writing – original draft. Yahui Xu: Funding acquisition, Supervision. Xinyi Wang: Investigation, Validation. Haozu Cheng: Investigation, Data curation, Validation.

Funding: This research was financially supported by the Key Research and Development Projects Fund of Henan Province (No. 231111320200).

Informed Consent Statement: All authors have read, understood, and have complied as applicable with the statement on "Ethical responsibilities of Authors" as found in the Instructions for Authors.

Acknowledgments: This research was financially supported by the Key Research and Development Projects Fund of Henan Province (No. 231111320200). This work was also supported by the Field Observation Station for Eco-Hydrological Processes in the Lower Yellow River Floodplain, Ministry of Water Resources. We are grateful for their data support and research facilities

Conflicts of Interest: The authors declare that they have no known competing financial interests or personal relationships that could have appeared to influence the work reported in this paper.

REFERENCES

1. Adnan, Muhammad., Xiao, Baohua., Xiao, Peiwen., Zhao, Peng., & Bibi, Shaheen. J. S. 2022. Heavy metal, waste, COVID-19, and rapid industrialization in this modern era—Fit for sustainable future. Sustainability, 14(8), 4746. https://doi.org/10.3390/su14084746.
2. Anderson, M.P.; Cherry, J.A. 1979. Using models to simulate the movement of contaminants through groundwater flow systems. Crit. Rev. Environ. Sci. Technol. 9, 97–156. https://doi.org/10.1080/10643387909381669.
3. Bai, Bing., Chen, Jing., Zhang, Bixia., & Wang, Hao. J. A. A. 2024. Migration trajectories and blocking effect of the fine particles in porous media based on particle flow simulation. AIP Advances, 14(4). https://doi.org/10.1063/5.0199046
4. Banaei, S.M.A.; Javid, A.H.; Hassani, A.H. 2021 Numerical simulation of groundwater contaminant transport in porous media. Int. J. Environ. Sci. Technol. 18, 151–162. https://doi.org/10.1007/s13762-020-02825-7.
5. Cao, Shiyuan., Sohn, Il., & Wang, Zhanjun. J. J. o. E. C. E. 2024. Selective stabilization of chromium and sustainable treatment of stainless steel slags. Journal of Environmental Chemical Engineering, 12(5), 113516. https://doi.org/10.1016/j.jece.2024.113516
6. Costabile, P.; Costanzo, C.; De Bartolo, S.; Gangi, F.; Macchione, F.; Tomasicchio, G.R. 2019. Hydraulic characterization of river networks based on flow patterns simulated by 2-D shallow water modeling: Scaling properties, multifractal interpretation, and perspectives for channel heads detection. Water Resour. Res. 55, 7717–7752. https://doi.org/10.1029/2018wr024083.
7. Cao, Y.; Dong, S.; Dai, Z.; Zhu, L.; Xiao, T.; Zhang, X.; Yin, S.; Soltanian, M.R. 2021. Adsorption model identification for chromium (VI) transport in unconsolidated sediments. J. Hydrol., 598, 126228. https://doi.org/10.1016/j.jhydrol.2021.126228.

8. De Smedt, F. 2016. Two-and three-dimensional flow of groundwater. In The Handbook of Groundwater Engineering; CRC Press: Boca Raton, FL, USA, pp. 121–144.
9. Dhal, B., Thatoi, H.N., Das, N.N., & Pandey, B.D. J. J. o. h. m. 2013. Chemical and microbial remediation of hexavalent chromium from contaminated soil and mining/metallurgical solid waste: a review. Journal of Hazardous Materials, 250, 272-291. https://doi.org/ 10.1016/j.jhazmat.2013.01.048
10. He, T.; Li, Y.; Huang, Y.; He, E.; Li, Y.; Qu, L.; Ding, F.; Jin, R.; Han, M.; Yuan, L.; et al. 2023. Simulation and risk assessment of arsenic by Hydrus-3D and CalTOX in a typical brownfield site. J. Hazard. Mater. 448, 130892. https://doi.org/10.1016/j.jhazmat.2023.130892.
11. He, Y.; Hu, G.; Zhang, Z.; Lou, W.; Zou, Y.; Li, X.; Zhang, K. 2022. Experimental study and numerical simulation on the migration and transformation mechanism of hexavalent chromium in contaminated site . J. Hazard. Mater. 43, 528–538. https://doi.org/10.16285/j.rsm.2021.6255.
12. Healy, R.W.; Scarlon, B.R. 2010. Estimating Groundwater Recharge; Cambridge University Press: Cambridge, UK ,.https://doi.org/10.1017/CB09780511780745.
13. Ghanbarian-Alavijeh, B.; Liaghat, A.; Huang, G.-H.; VAN Genuchten, M.T. 2010. Estimation of the van Genuchten Soil Water Re-tention Properties from Soil Textural Data. Pedosphere 20, 456–465. https://doi.org/10.1016/S1002-0160(10)60035-5
14. Liu, Peijun., Liu, Zhenggen., Chu, Mansheng., Yan, Ruijun., Li, Feng., Tang, Jue.,. Protection, E. 2022. Detoxification and comprehensive recovery of stainless steel dust and chromium containing slag: Synergistic reduction mechanism and process parameter optimization. Process Safety and Environmental Protection, 164, 678-695. https://doi.org/10.1016/j.psep.2022.06.034
15. Li, Xu., Wen, Zhang., Zhan, Hongbin., Wu, Fuxian., Zhu, Qi. J. E. S., & Research, P. 2021. Laboratory observations for two-dimensional solute transport in an aquifer-aquitard system. Environmental Science and Pollution Research, 28, 38664-38678. https://doi.org/10.1007/s11356-021-13123-1
16. Liang, X.; Zhang, Y.; Liu, J.; Ma, E.; Zheng, C. 2019. Solute transport with linear reactions in porous media with layered structure: A semianalytical model. Water Resour. Res. 55, 5102–5118. https://doi.org/10.1029/2019wr024778.
17. Paolina Bongioannini Cerlini.; Silvestri, L.; Meniconi, S.; Brunone, B. 2023. Performance of three reanalyses in simulating the water table elevation in different shallow unconfined aquifers in central Italy. Meteorol. Appl. 30, e2118. https://doi.org/10.1002/met.2118.
18. Qiao, Pengwei., Wang, Shuo., Li, Jiabin., Zhao, Qianyun., Wei, Yan., Lei, Mei., .Zhang, Zhongguo. J. S. o. t. T. E. 2023. Process, influencing factors, and simulation of the lateral transport of heavy metals in surface runoff in a mining area driven by rainfall: A review. Science of The Total Environment, 857, 159119.
19. Sumit, Shukla, R., & Sinha, A. K. J. S. 2021. Finite element method coupled with TLBO for shape control optimization of piezoelectric bimorph in COMSOL Multiphysics. SIMULATION, 97(9), 635-644. https://doi.org/10.1177/00375497211025640
20. Sathe, S.S.; Mahanta, C. 2019. Groundwater flow and arsenic contamination transport modeling for a multi aquifer terrain: As-sessment and mitigation strategies. J. Environ. Manag. 231, 166–181. https://doi.org/10.1016/j.jenvman.2018.08.057.
21. Song, X.; Borja, R.I. 2014. Mathematical framework for unsaturated flow in the finite deformation range. Int. J. Numer. Methods Eng. 97, 658–682. https://doi.org/10.1002/nme.4605.

22. Therrien, R.; Sudicky, E.A. 1996. Three-dimensional analysis of variably-saturated flow and solute transport in discretely-fractured porous media. J. Contam. Hydrol., 23, 1–44. https://doi.org/10.1016/0169-7722(95)00088-7.
23. Thanh, N.N.; Thunyawatcharakul, P.; Ngu, N.H.; Chotpantarat, S. 2022. Global review of groundwater potential models in the last decade: Parameters, model techniques, and validation. J. Hydrol. 614, 128501. https://doi.org/10.1016/j.jhydrol.2022.128501.
24. Tian-chyi, J. Y.; Mao, D.-Q.; Zha, Y.-Y.; Wen, J.-C.; Wan, L.; Hsu, K.-C.; Lee, C.-H. 2015. Uniqueness, scale, and resolution issues in groundwater model parameter identification. Water Sci. Eng. 8, 175–194. https://doi.org/10.1016/j.wse.2015.08.002.
25. Xu, Hong.-Bin., Zhang, Yi., Li, Zuo.-Hu., Zheng, Shi.-Li., Wang, Zhi.-Kuan., Qi, Tao., & Li, Hui.-Quan. J. J. o. C. P. 2006. Development of a new cleaner production process for producing chromic oxide from chromite ore. Journal of Cleaner Production, 14(2), 211-219. https://doi.org/10.1016/j.jclepro.2004.09.001
26. Xie, Chengyu., Qin, Yaguang., Chao, Lei., & Shi, Dongping. J. A. A. 2020. Applied research on the numerical simulation of Cu and Cd transport laws in a metal mining area. AIP Advances, 10(11). https://doi.org/10.1063/5.0025590
27. Yang, X.; Xi, G.; Yao, N.; Zhou, M.; Gao, X.; Chen, M.; Wang, X.; Pan, Z.; Wang, Z. 2022. Spatiotemporal distribution of residual ammonium in a rare-earth mine after in-situ leaching: A modeling study with scarce data. J. Hydrol. 615, 128669. https://doi.org/10.1016/j.jhydrol.2022.128669.
28. Yan, C. Numerical Simulation of Groundwater Pollutant Transport in Phosphogypsum Dump. Thesis, 2019. https://doi.org/10.27671/d.cnki.gcjtc.2019.000559.
29. Wang, R.; Zhang, Y.; Chen, W.; Shao, J.; Cui, Y.; Zhang, Q. 2025. Chromium Migration in Contaminated Site and Numerical Simulation of Its Effect on Groundwater Source Area. Rock Miner. Anal. 1–14, https://doi.org/10.15898/j.ykcs.202409110189.
30. Wan, P.; Zhou, L. 2021. Simulation of the migration and transformation of total phosphorus in groundwater during a certain phosphate mine mining period based on GMS. Nonferrous Met. (Min. Sect.) 73, 117–122. https://doi.org/10.3963/j.
31. Wang, J.; Yang, Z.; Chen, J.; Wang, Z. 2000. Study on soil moisture retention characteristics in aeration zone. J. Hydraul. Eng. 1–6. https://doi.org/10.13243/j.cnki.slxb.2000.02.001. (In Chinese)
32. Zhang, Wenbing., Shen, Zhenzhong., Ren, Jin., Gan, Lei., Wang, Fei., Yu, Bihan., & Li, Chenglin. J. J. o. H. 2020. Modeling and comparative analysis of a flow and heat coupling model of the riparian zone based on thermal conductivity empirical models. Journal of Hydrology, 582, 124539. https://doi.org/10.1016/j.jhydrol.2019.124539